Pergamon

Int. J. Heat Mass Transfer. Vol. 39, No. 18, pp. 3835–3844, 1996
Copyright © 1996 Elsevier Science Ltd
Printed in Great Britain. All rights reserved
0017–9310/96 $15.00+0.00

PII: S0017–9310(96)00043–9

Ultra-shallow p^+-junction formation in silicon by excimer laser doping: a heat and mass transfer perspective

X. ZHANG, J. R. HO and C. P. GRIGOROPOULOS†
Department of Mechanical Engineering, University of California, Berkeley, CA 94720, U.S.A.

(*Received* 10 *November* 1995 *and in final form* 30 *January* 1996)

Abstract—Heat and mass transfer at the nanosecond time scale and the nanometer length scale in pulsed laser fabrication of ultra-shallow p^+-junctions is studied in this work. A new technique is developed to fabricate the ultra-shallow p^+-junctions with pulsed laser doping of crystalline silicon with a solid spin-on-glass (SOG) dopant, through the nanosecond pulsed laser heating, melting, and boron mass diffusion in the 100 nm thin silicon layer close to the surface. High boron concentration of 10^{20} atoms cc^{-1} and the 'box-like' junction profile are achieved. The key mechanism determining the 'box-like' junction shape is found to be the melt–solid interface limited diffusion. The ultra-shallow p^+-junctions with the depth from 30 to 400 nm are successfully made by the excimer laser. The optimal laser fluence condition for SOG doping is found about 0.6–0.8 J cm^{-2} by studying the ultra-shallow p^+-junction boron profiles measured by the secondary ion mass spectroscopy (SIMS) vs the laser fluence and the pulse number. The one-dimensional numerical analysis agrees reasonably with the experiment, within the available physical picture. Possible mechanisms such as boron diffusivity dependence on the dopant concentration in the molten silicon are proposed. Copyright © 1996 Elsevier Science Ltd.

1. INTRODUCTION

With today's rapid development in sub-micron electronics, it is becoming increasingly urgent to fabricate a high concentration ultra-shallow p^+-junction for the source and drain of the PMOS (*p*-channel metal-oxide-semiconductor) transistor [1]. This need presents a challenge to current semiconductor doping technologies such as the furnace diffusion and the ion implantation. It is difficult to achieve both high concentration and ultra-shallow junctions by the conventional furnace doping due to the nature of the solid phase diffusion and the lack of controllability, even though many efforts have been made towards developing RTP (rapid thermal process) techniques [2]. On the other hand, by the ion implantation technique that has been extensively studied and implemented in the current semiconductor industry, one is still unable to form high concentration ultra-shallow p^+-junctions. The insurmountable obstacles arise because the required very low ion implantation energies reach the limit of the implantation equipment capabilities and from the greater inherent channeling effect in crystalline silicon for the light ions such as boron [3, 4]. A modified ion implantation method has been developed to amorphize the silicon wafer surface first, in order to reduce the boron channeling in the implantation process. However, several post-anneals are needed and defects are often generated within the junctions, degrading device performance [5, 6].

To meet the mandatory requirements of both high doping concentration and ultra-shallow junction depth for PMOS, it is necessary to explore new techniques. It would be interesting then to seek new techniques that can generate the transformation to the liquid silicon phase, where the boron diffusivity is extremely high, thus enabling easier and more precise control of the diffusion time. The pulsed u.v. excimer laser as an intensive heating source can provide a new avenue. With the peak power as high as 10^8 W, the excimer laser light can be strongly absorbed by the silicon surface within a depth of 10 nm, resulting in a thin molten silicon layer near the surface. Since the boron mass diffusivity in liquid silicon is by six orders of magnitude larger than that in solid silicon, excimer laser irradiation can confine the diffusion within the thin molten silicon layer at the nanosecond time scale. By controlling the laser pulse energy, the thickness of the thin molten silicon layer can be incrementally changed from a few nanometers to microns. Therefore, it is possible to precisely control the maximum diffusion depth. Also the short pulse width of the excimer laser, which is of the order of 10 ns, provides a complementary way of adjusting the diffusion zone within the molten silicon layer by varying the number of laser pulses, thereby essentially changing the mass diffusion time. Meanwhile, the high boron diffusivity in the thin liquid silicon layer results in a very high doping concentration in the region. A gas immersion layer doping process (GILD) has been developed [7],

† Author to whom correspondence should be addressed.

NOMENCLATURE

C	dopant concentration
C_0	surface dopant concentration
C_p	thermal capacity
d_1	thickness of the silicon wafer
d_2	thickness of the thin dopant SOG film
D	mass diffusivity
d_j	junction depth
Δd_j	junction transition depth
h	enthalpy
i	imaginary unit ($= \sqrt{-1}$)
I	laser intensity
k	thermal conductivity
N	laser pulse number
N_p	total number of grid points in the computational domain
$\bar{n}_1$	complex refractive index of SOG thin film
$\bar{n}_2$	complex refractive index of silicon substrate
Q_{ab}	laser intensity absorbed by the crystalline silicon
r_1	reflection coefficient at air–film interface
r_2	reflection coefficient at film–substrate interface
R	reflectivity of the sample at $\lambda = 248$ nm
t	time
T	temperature
T_r	room temperature
z	coordinate perpendicular to silicon surface.

Greek symbols

α	absorption coefficient
λ	laser wavelength
ρ	mass density.

in which dopant gas molecules such as BCl_3 and PCl_3 are dissociated upon the u.v. laser irradiation and incorporated into the think molten silicon layer. It has been demonstrated that submicron shallow junctions can be formed by this gas phase laser doping technique and good device characteristics have been achieved [8–10]. However, the gas phase immersion laser doping requires a sophisticated vacuum chamber and mass flow control systems. Solid-state dopants have been traditionally used in a furnace diffusion process for semiconductor device fabrication, because of its simplicity. In this work, a new technique is developed for fabrication of the ultra-shallow p^+-junction by the excimer laser doping of crystalline silicon with a solid dopant spin-on-glass (SOG) film. By using solid dopants in excimer laser doping, not only does the process itself become simple, but also the laser energy coupling into the silicon wafer can be enhanced up to two times due to the thin film interference effect. The boron dopant profiles in the thin layer near the silicon surface, which depend on the excimer laser fluence and the pulse number, are obtained by the secondary ion mass spectroscopy (SIMS). The rapid transient heat transfer and mass transfer in the thin molten silicon layer induced by laser heating are studied, at the time scale of nanoseconds and the length scale of nanometers. Numerical simulations are conducted to compare with the experimental dopant profiles. The p^+-junction depth and sharpness as functions of laser fluence and pulse number are revealed.

2. EXPERIMENT

The sample structure is shown in Fig. 1. Upon the excimer laser irradiation, the thin layer near the silicon surface is rapidly heated and melting starts as the surface reaches the silicon melting temperature of 1685 K. The melting turns on the boron diffusion in the liquid silicon immediately. After the melting front reaches the maximum depth, the solidification limits the boron diffusion process at the solidification front. The sample is prepared in a clean room environment at the Microfabrication Laboratory at the University of California at Berkeley. A 4-in n-type (100) CZ silicon prime wafer with the resistivity of 5–10 Ω-cm is used for the laser doping experiment. The wafer is cleaned through the standard process by a Piranha solution and rinsed in DI water tanks. The native silicon dioxide on the wafer surface is removed by a diluted 10:1 HF solution. After 1 h baking at 120°C, the wafer is coated with the boron doped spin-on-glass with dopant concentration 2×10^{21} cc^{-1} by spinning the glass solution at 3000 rpm. The sample is then baked on a hot plate at 250°C for 2 h to drive out the residue solvents inside the thin glass film. The thickness of the dopant glass film is designed as 3000 Å in this experiment to enhance the laser energy coupling into the silicon at KrF laser wavelength $\lambda = 248$ nm based on the thin film interference effect. The dopant film thickness is measured as 3050 Å by the Gaertner L116A ellipsometer and the Nanospec interferometer. A separate dopant film is spun on a quartz wafer and optical transmission is measured about 95% at 248 nm. Therefore, the film can be treated as transparent. The thickness uniformity of the thin film dopant glass is found to be better than $\pm 5\%$ across the wafer.

The experimental setup for the excimer laser doping is shown in Fig. 2. A Lumonics Index 200 excimer laser with the wavelength of 248 nm and pulse width of 26 ns (FWHM) is used as a heating source to induce

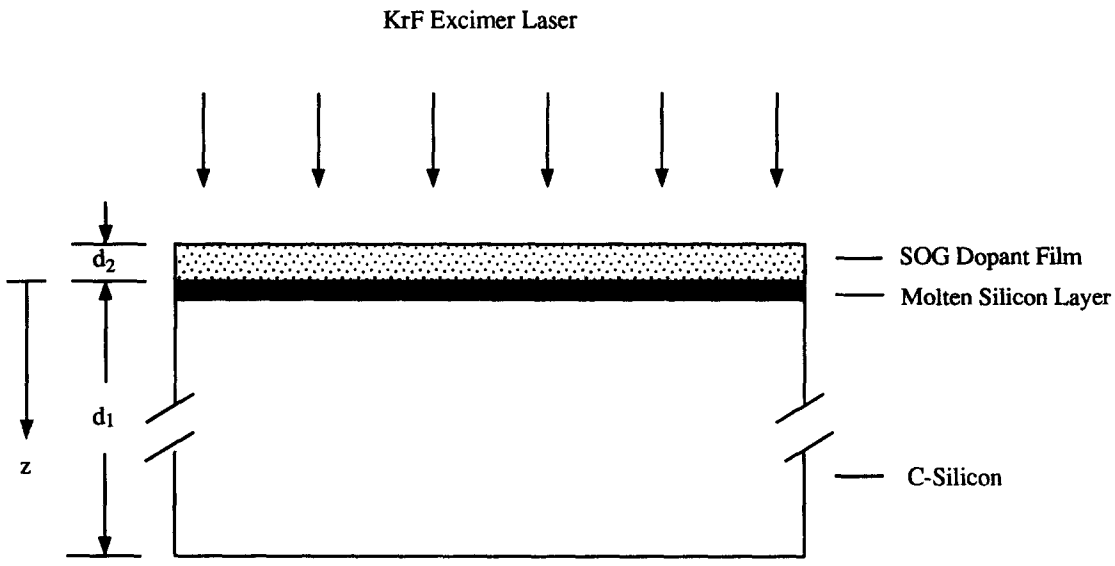

Fig. 1. Schematic sample structure for the ultra-shallow p^+-junction formation by the excimer laser doping with a solid dopant spin-on-glass.

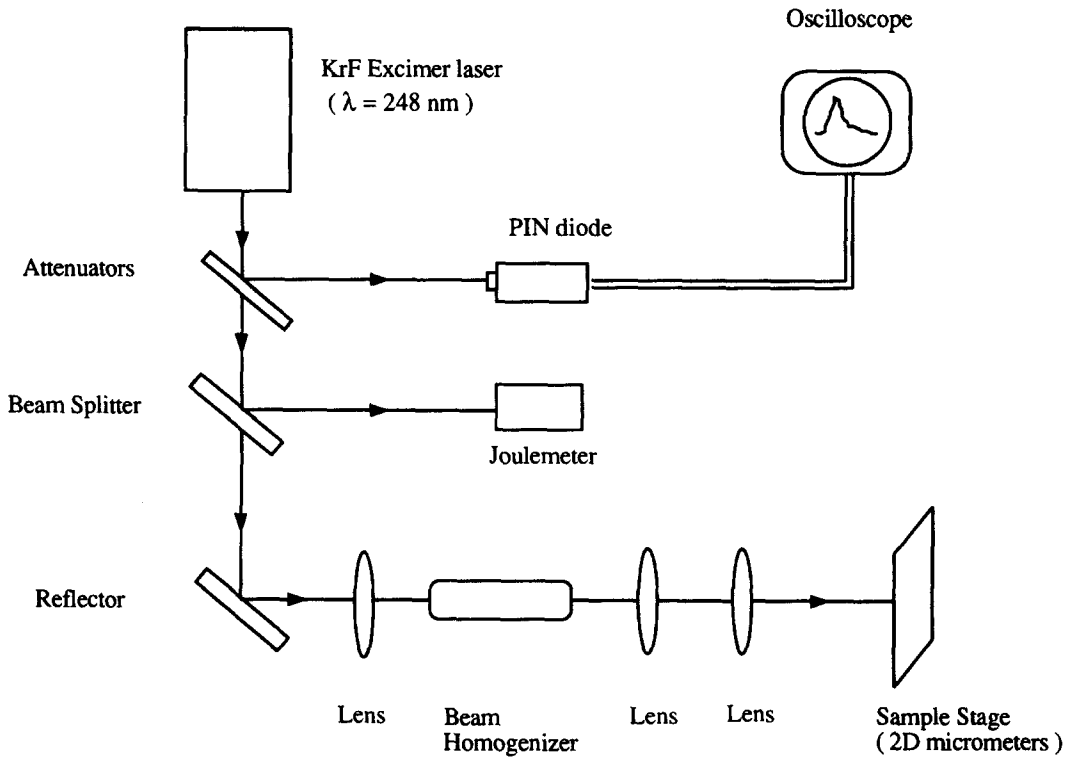

Fig. 2. Schematic experimental set-up for the excimer laser doping of the silicon dopant spin-on-glass.

the thin melting layer on the silicon surface. The pulsed laser beam is delivered through a set of optics that includes a beam homogenizer, mirrors and transfer lenses. The optical alignment is performed to ensure the system optimization and the laser spot profile uniformity on the silicon wafer. The laser fluence on the silicon wafer surface is varied by changing the excimer laser electrode voltage and by using a set of laser beam attenuators. The sample is translated through an X–Y micrometer stage. The laser pulse energy is monitored by the molectron joulemeter detecting the 10% laser beam reflected at a beam splitter, while the 90% transmitted beam is focused on the sample. The temporal laser intensity profiles are recorded by a silicon *PIN* photodiode at a HP 54510A digitizing oscilloscope with nanosecond resolution. The laser fluences studied in this work range from 0.6 J cm^{-2} which is close to the silicon melting

threshold, to 0.9 J cm^{-2} where the surface temperature of molten silicon layer is still below the oxide dopant film melting point of 1980 K. Therefore, the oxide dopant film stays in the solid phase during the silicon melting process. In order to study the transient thermal and mass diffusion in the thin liquid silicon layer and optimize the process to achieve the 'box-like' dopant profile in the p^+-junction, the laser pulse number N for each fixed laser fluence is chosen as 1, 5, 10 and 20, respectively. After the laser doping, the dopant glass layer is etched away at a diluted 10:1 HF solution. Several rinses are necessary to ensure that the silicon surface is free from contaminants.

The boron dopant depth profiles are measured with the Phi 660 SEM-AUGER-SIMS system with the vacuum of 2×10^{-9} torr. The sample surface morphology is examined by the scanning electron microscope (SEM). A liquid gallium ion beam with a diameter of 2 μm is used for sputtering by scanning an area of 50×50 μm or 100×100 μm on the laser doped p^+-junction region. A quadrupole mass spectrometer analyzes the sputtered material from the p^+-junction sample and counts the boron ions instantaneously with the sputtered depth into the sample. Ion gun alignment is carried out to ensure both the gallium ion beam and the mass spectrometer are focused at the same area on the sample. A boron-implanted silicon reference sample from the Charles Evans Associates (Redwood City, CA) is used for calibration of the boron concentration in the p^+-junctions fabricated in this work. The calibration is performed at the same SIMS (secondary ion mass spectroscopy) operation conditions such as the magnification and the gallium ion current [11]. The depth calibration is done by measuring the sputtered crater depth in the reference sample at the Tencor Alpha-Step 200 surface profilometer.

3. NUMERICAL SIMULATION

In order to understand the heat and the mass transfer in the ultra-shallow p^+-junction formation under the excimer laser irradiation on the silicon wafer with a thin solid diffusion oxide film, a one-dimensional numerical analysis is developed to simulate the transient heat and mass diffusion of the boron atoms across the thin molten silicon layer. The laser energy intensity absorbed by the silicon, Q_{ab}, is represented as a volumetric source term in the energy equation, as is given by

$$Q_{ab}(z,t) = (1-R)I(t)\alpha\exp(-\alpha z) \tag{1a}$$

$$R = \left|\frac{r_1 + r_2\exp(-i4\pi\bar{n}_1 d_2/\lambda)}{1 + r_1 r_2\exp(-i4\pi\bar{n}_1 d_2/\lambda)}\right|^2, \tag{1b}$$

where R is the reflectivity of the thin SOG film on the silicon substrate and α is the absorption coefficient of the silicon at laser wavelength $\lambda = 248$ nm. d_2 is the thickness of the film which is 3050 Å. r_1 and r_2 are reflection coefficients containing refractive indices of $\bar{n}_1 = (1.5, 0)$ and $\bar{n}_2 = (3.58, 1.68)$ for the dopant film and silicon substrate, respectively. Taking advantage of the thin film interference effect, the reflectivity from the sample can be reduced from 0.67 for bare silicon to 0.56 for the SOG thin film on crystalline silicon substrate. Therefore, the laser energy coupling into silicon substrate is increased by 17%. The 100% enhancement in laser energy coupling into the sample can be achieved by carefully designed thin film thickness for the devices manufacturing environment. The distance from the wafer surface into the silicon z is defined in Fig. 1. The laser absorption depth is of the order of 10 nm and the thermal penetration depth is about a few microns in solid silicon, while the cross-section of the laser beam is of the order of millimeter. Thus, the heat transfer in the silicon can be approximated as a one-dimensional conduction problem described by

$$(\rho C_p)(T)\frac{\partial T}{\partial t} = \frac{\partial}{\partial z}\left(k(T)\frac{\partial T}{\partial z}\right) + Q_{ab}. \tag{2}$$

Two boundary conditions and an initial condition are required

$$T(z=d_1,t) = T_\infty, \quad \frac{\partial T}{\partial z}(z=-d_2,t) = 0,$$
$$T(z,t=0) = T_\infty \tag{3}$$

where d_1 and d_2 are thicknesses of the silicon wafer and the dopant SOG film, respectively, shown in Fig. 1. T_∞ is the room temperature. The heat conduction equation, in the enthalpy formulation for the solution of phase change problems [12, 13], can be written as

$$\frac{\partial h(T)}{\partial t} = \frac{\partial}{\partial z}\left(k(T)\frac{\partial T}{\partial z}\right) + Q_{ab}, \tag{4}$$

where the enthalpy h is a function of temperature, $h = h(T)$. The enthalpy equation and the associated BCs and IC are discretized using the Crank–Nicolson formulation incorporating temperature-dependent material properties. A nonuniform grid system is used in the computational domain. The maximum grid size for the possible melting regime was set smaller than 10^{-11} m. At each time step, the numerical solution is iterated upon, with the convergence criterion set as

$$\max\left|\frac{T_i^{new} - T_i^{old}}{T_i^{old}}\right| \leqslant 10^{-10} \quad \text{for } i = 1, N \tag{5}$$

where the subscript i denotes the grid position, the superscripts new and old represent the consequent two iterations. N_p indicates the total number of grid points in the computation domain.

As a first-order approximation, the thermal properties are independent of the concentration and the mass diffusivity in the molten silicon layer is independent of the temperature. Therefore, the mass diffusion is decoupled from the thermal equations. The mass

diffusion can be solved numerically at each time step after the temperature field and melt–solid interface are found. Transient boron mass diffusion in this work is modeled by the one dimensional Fick's equation

$$\frac{\partial C}{\partial t} = \frac{\partial}{\partial z}\left(D\frac{\partial C}{\partial z}\right). \quad (6)$$

The boundary conditions and the initial condition for the mass transport are given by

$$C(z=0,t) = C_0 \quad C(Z=d_2,t) = 0 \quad C(z,t=0) = 0 \quad (7)$$

where the surface boron concentration C_0 is chosen as the experimentally measured value. Since the dopant concentration is about 2×10^{21} cc^{-1} in SOG film and the boron solubility in silicon is about order of 10^{20} cc^{-1}, the amount of boron diffused into the silicon at this work does not exceed 5% of the total dopant in the SOG film. Therefore, the surface of the silicon can be treated as saturated at a constant concentration C_0, which agrees with experimental observations described in the following section. Boron diffusivity D is set as a constant 2.3×10^{-4} cm^2 s^{-1} in liquid silicon [14] and zero in solid due to the six orders of magnitude difference between the mass diffusivities in the two phases. The thermal properties and mass diffusivities used in numerical simulation are listed in Table 1.

4. RESULTS AND DISCUSSION

The morphology of the laser doped p^+-junction region after the removal of thin SOG layer is smooth, as shown in Fig. 3 by the scanning electron microscopy (SEM). Smaller scale SEM also shows no surface topography generation. This suggests that the one-dimensional heat and mass transfer approach in both a solid and molten silicon thin layer is reasonable. The thin oxide dopant film actually helps to stabilize the molten surface during the transient melting, while the boron atoms diffuse into the melt. However, at this point, it is not clear yet whether the molten silicon solidification process is epitaxial for the laser fluences in the range of 0.6–0.9 J cm^{-2}. The microstructure generated in the recrystallized junction region plays an important role in the heat and mass transfer driven by the following pulses, because of the possible changes in the physical properties of the surface layer [15]. Ultimately, this affects the p^+-junction quality.

Boron dopant concentration profiles at a fixed energy 700 mJ cm^{-2}, are shown in Fig. 4. p^+-Junctions with depth of 70 to 140 nm are successfully fabricated. The boron concentration as high as 2×10^{20} atoms cc^{-1} is obtained, which is about the boron solubility in crystalline silicon. Such a high doping level is mainly due to the high boron mass diffusivity in the thin liquid silicon layer induced by the pulsed laser irradiation. The diffusion profiles extend further into the thin molten silicon as the laser pulse number increases, although the highest concentration is upbound by the boron solubility. It is interesting that, as the laser pulse number increases, the dopant profile shape is more 'box-like' rather than the gradual decrease observed in most diffusion cases. The abrupt or 'box-like' dopant profiles render the ideal p^+-junction properties [8]. The art in the formation of this 'box-like' shape lies on the fact that, as the pulse number increases, the boron diffusion is limited by the maximum melting depth determined by the pulsed laser energy and pulse width. After the boron diffusion reaches the maximum melting depth, more boron atoms are piled up and accumulated in the molten layer instead of crossing the melt–solid interface, because of the very low boron diffusivity in the solid silicon. At 20 laser pulses, almost the entire thin molten layer of 140 nm thickness is saturated with boron dopant. It is also demonstrated that the p^+-junction depth can be incrementally changed by varying the laser pulse number at a fixed laser fluence. Numerical simulation based on a one-dimensional transient thermal and mass diffusion model predicts similar p^+-junction profiles. Both the experimental and numerical dopant profiles at larger pulse numbers coincide to a certain depth of about 140 nm, which is found through computation to be the maximum

Table 1. Thermal properties and mass diffusivities used in numerical simulation of ultrashallow p^+-junction formation

Melting temperature [K]	$T_m = 1685$	Si
	$= 1980$	SOG (SiO_2)
Density [kg m^{-3}]	$\rho = 2.33\times10^3$	Solid Si
	$= 2.52\times10^3$	Liquid Si
	$= 2.2\times10^3$	SOG (SiO_2)
Thermal conductivity [W m^{-1} K^{-1}]	$k(T) = 2.99\times10^4/(T-99)$	Solid Si
	$= 67$	Liquid Si
	$= 1.39$	SOG (SiO_2)
Thermal capacity [J kg^{-1} K^{-1}]	$C_p = (1.4743+5.689\times10^{-4}T)\times10^6/\rho$	Solid Si
	$= 9.6045\times10^2$	Liquid Si
	$= 740$	SOG (SiO_2)
Boron diffusivity [cm^2 s^{-1}]	$D = 0$	Solid Si
	$= 2.3\times10^{-4}$	Liquid Si
Latent heat [J kg^{-1}]	$\Delta h = 1.4\times10^6$	Silicon

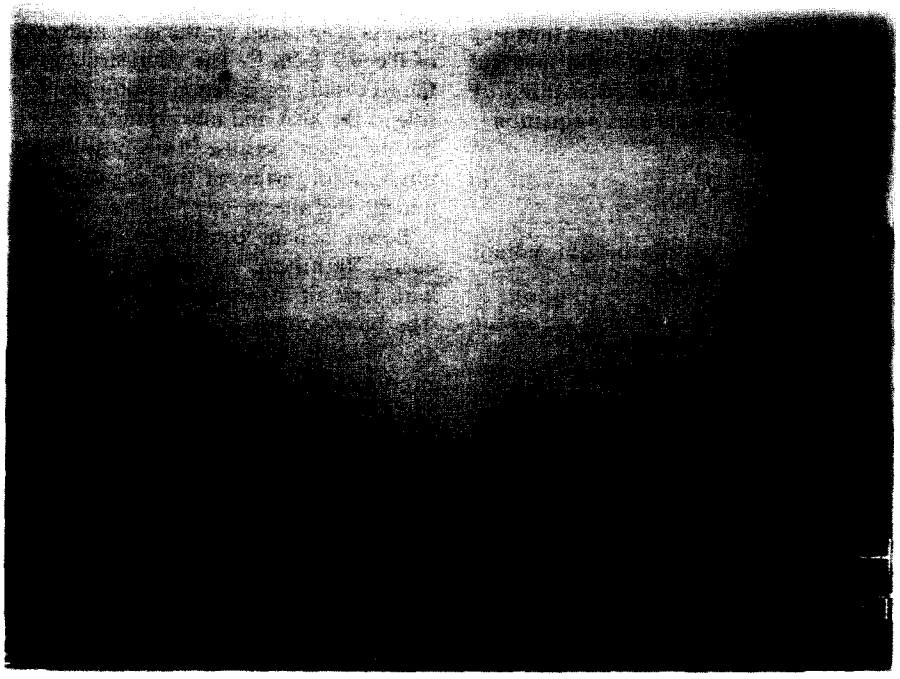

Fig. 3. Ultra-shallow p^+-junction surface morphology imaged by a scanning electron microscopy (SEM).

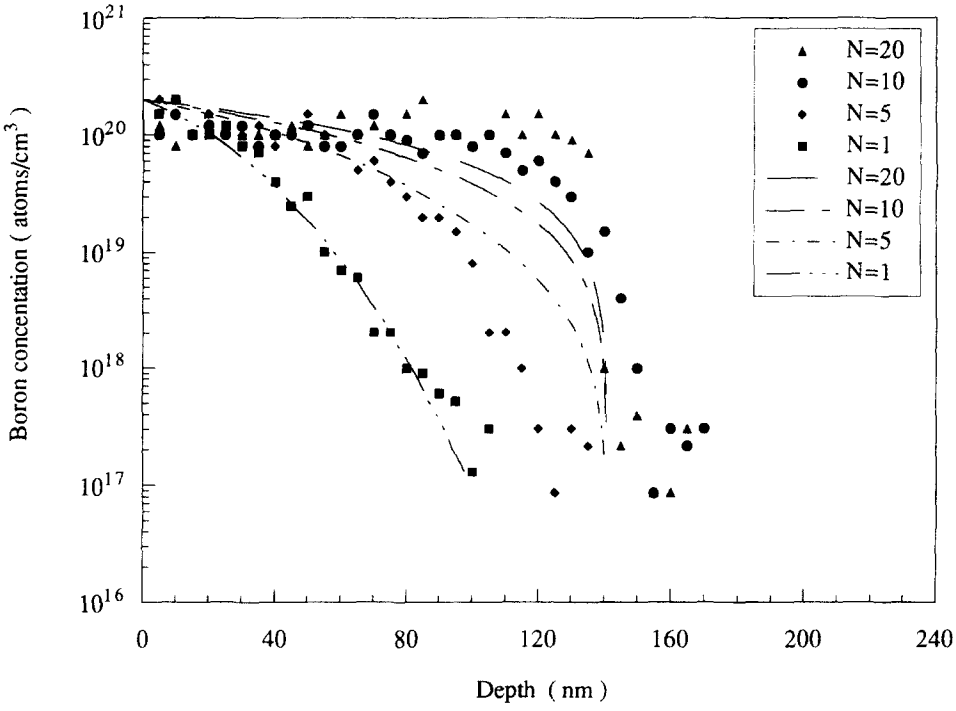

Fig. 4. Ultra-shallow p^+-junction dopant concentration depth profiles at different laser pulse number N with a fixed laser fluence 0.7 cm^{-2}. The solid dots are experimental data measured by the second ion mass spectroscopy (SIMS) and the lines are numerical results.

melting depth at the laser fluence of 700 mJ cm^{-2}. The computational results fit the experimental profile well for the first laser pulse, but deviate substantially as the pulse number N increases. Numerically predicted dopant concentrations are generally lower than the experimental ones. It is believed that the boron diffusivity may depend on the boron concentration if the region is heavily doped, compared with the silicon intrinsic carrier density of the order of 10^{19} cc^{-1} at the melting temperature [16]. For the first few pulses, the heavily doped region is so small that the effect from the concentration dependence of the boron diffusivity

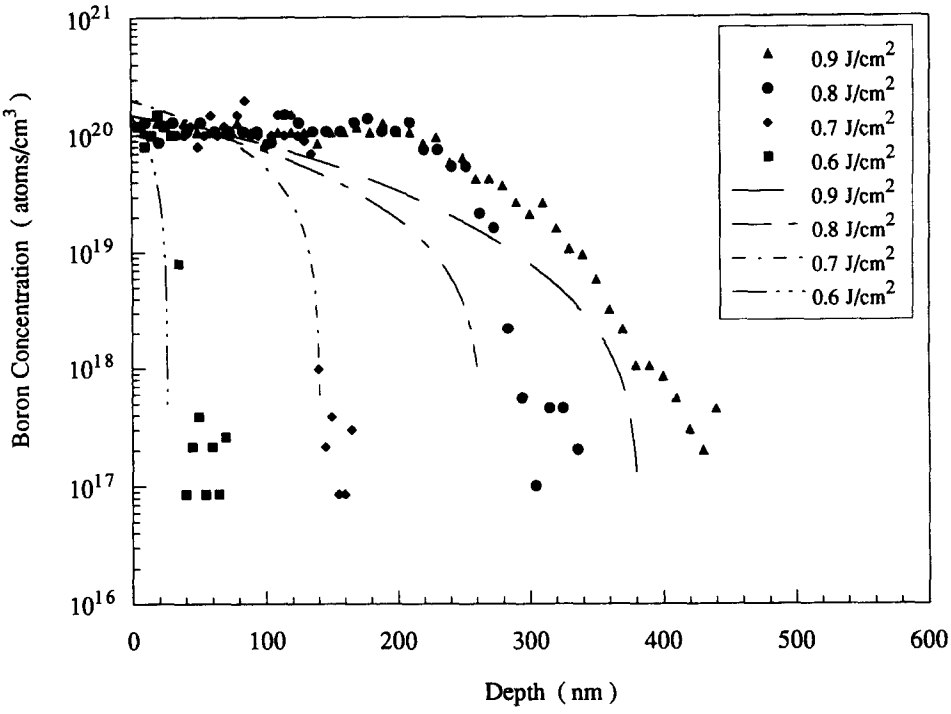

Fig. 5. Ultra-shallow p^+-junction dopant concentration depth profiles at different laser fluence with a fixed pulse number $N = 20$. The solid dots are experimental data measured by the second ion mass spectroscopy (SIMS) and the lines are numerical results.

is not significant. Boron diffusivity can be treated as a constant in the computations. As the pulse number increases, a larger fraction of the molten region becomes heavily doped, leading to a change in the boron diffusivity. A larger boron diffusivity could result in higher computed concentration for $N = 10$ and $N = 20$ in Fig. 4. There are other factors possibly causing the differences between the experimental profiles and numerical profiles at higher pulse numbers. First, the laser fluence measured by the Joulemeter is averaged over the pulses for the case of multiple laser pulses. Pulse to pulse fluence fluctuations generated by the excimer laser can be as large as 10%. The fluctuations can result in not only changes in the thermal process, but also in the mass diffusion. The final dopant profiles are affected more strongly by the higher fluence pulses than the lower ones during the multi-phase doping. Second, the microstructure in the resolidified thin layer is also of importance during the multi-pulse laser irradiation. Assuming epitaxial recrystallization in the thin liquid silicon layer, the numerical simulation in this work may not be accurate enough to predict the thermal transport due to possible changes in physical properties such as the thermal diffusivity in the recrystallized silicon. Third, the absorption coefficient of c-silicon may change due to the heavily doped silicon surface during multiple laser irradiation. Lastly, the thermal conductivity of solid silicon layer can be decreased by a factor of 2–5 in the temperature range from room temperature to 600 K because of the heavy doping with boron [17, 18]. At higher temperatures, the thermal conductivity becomes less affected by the high dopant concentration. The decrease in thermal conductivity can lead to deeper and longer melting in silicon. The 10% increase in the liquid silicon thermal conductivity from 1685 to 1980 K during the pulsed laser doping may also influence the transient thermal and mass transport [19].

Figure 5 shows boron dopant depth profiles for different laser fluences at a fixed pulse number $N = 20$. It is demonstrated that the p^+-junctions are 'box-like' for 0.6, 0.7 and 0.8 J cm^{-2}, but not for 0.9 J cm^{-2}. The difference can be explained by the maximum melting depth. For the fixed pulse number $N = 20$, the boron diffusion depths already exceed the maximum melting depth at the laser fluences 0.6, 0.7 and 0.8 J cm^{-2}. The accumulation of the dopant atoms blocked by the liquid–solid interface results in the 'box-like' dopant distributions. However, for the higher laser fluence like 0.9 J cm^{-2}, the diffusion penetration length at $N = 20$ is smaller than the maximum melting length and therefore, no dopant accumulation occurs. The p^+-junction depth increases with the laser fluence because of the increase in both the melting depth and the melting duration. By defining the p^+-junction depth d_j as the distance from the surface to the position where the concentration drops below 10^{18} cc^{-1}, the junction depths vs the laser fluences at two different pulse numbers $N = 1$ and $N = 20$ are shown in Fig. 6. The computed junction depths are plotted for comparison. The gradual saturation of the junction depths

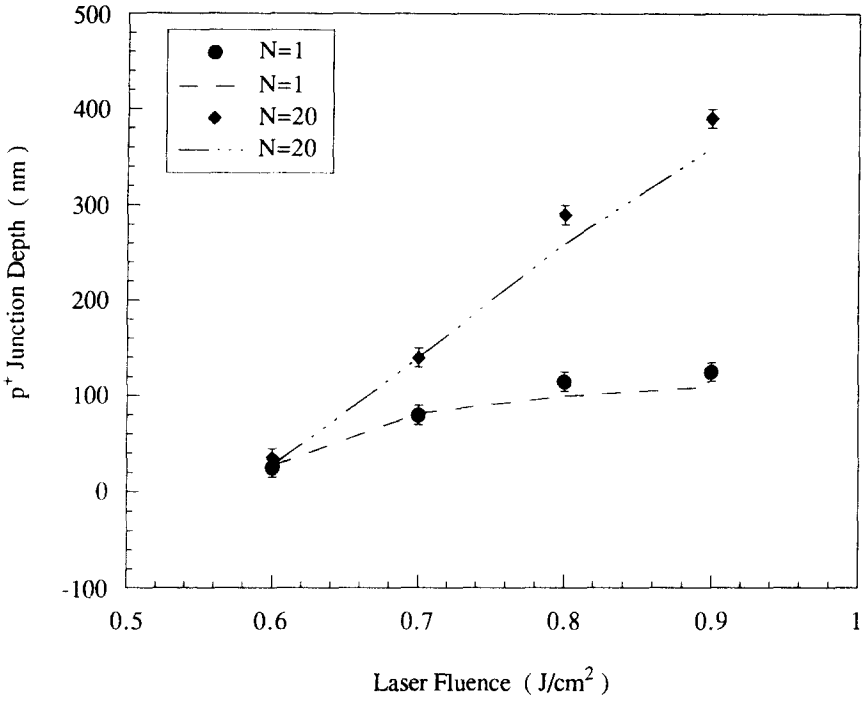

Fig. 6. Ultra-shallow p^+-junction depth dependence on the laser fluence for $N = 1$ and $N = 20$. The solid dots are experimental data measured by the second ion mass spectroscopy (SIMS) and the lines are numerical results.

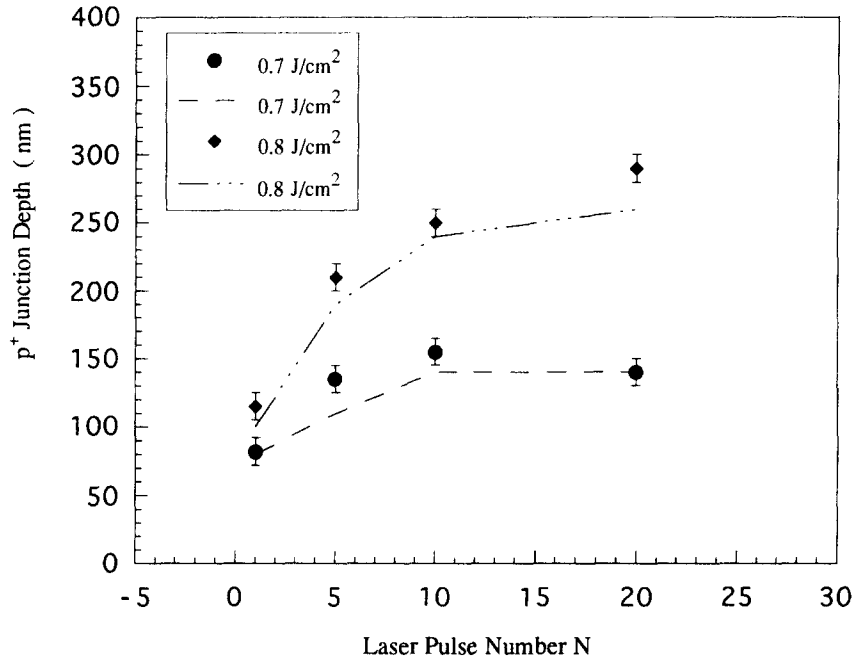

Fig. 7. Ultra-shallow p^+-junction depth dependence on the laser pulse number for laser fluences 0.7 and 0.8 J cm^{-2}. The solid dots are experimental data measured by the second ion mass spectroscopy (SIMS) and the lines are numerical results.

with the pulse number N at fixed laser fluences is observed in Fig. 7, which shows the melt–solid interface limited diffusion. The ultra-shallow p^+-junctions of 30 nm depth at the laser fluence of 0.6 J cm^{-2} are successfully fabricated with this spin-on-glass (SOG) pulsed laser doping technique. It is demonstrated that the incremental depth achieved by varying the pulse number N can be as small as 20–30 nm. However, by varying the laser fluence at an experimentally controllable level (about 0.1 J cm^{-2}), the incremental

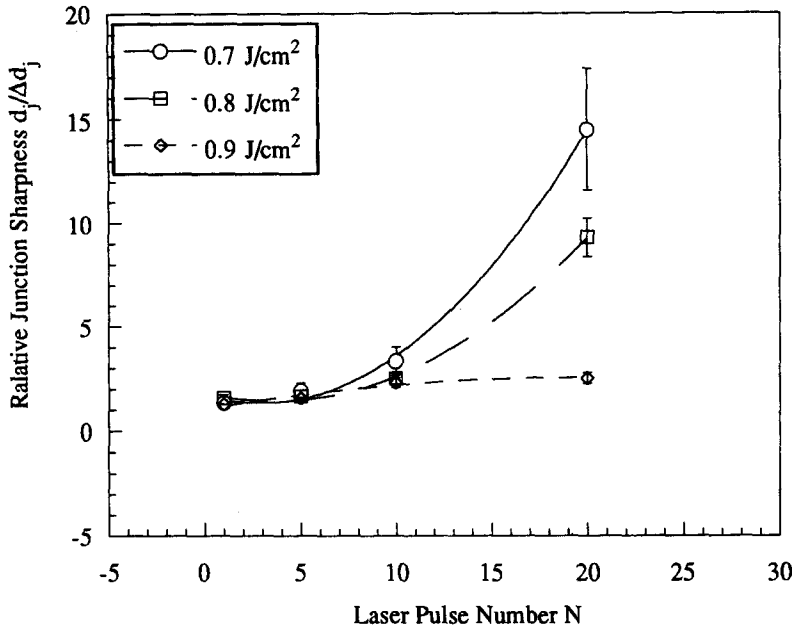

Fig. 8. Relative p^+-junction sharpness dependence on the laser pulse number at laser fluences as 0.6, 0.7, 0.8, 0.9 J cm^{-2}.

depth is relatively larger than that obtained by varying the pulse number because the melt depth is mainly dominated by the larger melting depth and longer melting duration. The p^+-junction sharpness is an important factor in the device performance. By defining the relative junction sharpness as $d_j/\Delta d_j$, where Δd_j is the junction transition depth, it is found that the p^+-junction sharpness increases rapidly as the pulse number N increases for the lower laser fluences of 0.6, 0.7 and 0.8 J cm^{-2}, as shown in Fig. 8. For the laser fluence of 0.9 J cm^{-2}, the p^+-junction sharpness grows much slower than the lower fluence cases due to the fact that the melting depth is longer than the diffusion depth up to 20 pulses, as mentioned earlier. Again, the melt–solid interface limited diffusion is confirmed in Fig. 8. The optimal fluence range in pulsed laser SOG doping is therefore positioned at about 0.6–0.8 J cm^{-2}.

The transient pulsed laser induced melting and diffusion in silicon is a complex phenomenon. Several factors, especially the physical properties of the thin silicon layer can be altered during the multiple laser pulses. It should be pointed out that the boron diffusivity dependence on the concentration and the temperature in the thin liquid silicon layer is not known yet.

5. CONCLUSIONS

Ultra-shallow p^+-junctions ranging from 30 to 400 nm are successfully fabricated by the pulsed excimer laser doping of crystalline silicon with a solid dopant film SOG. The idea is to melt a thin layer of silicon by the pulsed laser irradiation so that the diffusion can be confined within the thin liquid silicon layer, because of the much higher boron diffusivity in liquid silicon compared with that in solid silicon. The p^+-junction depth is essentially controlled by the pulsed laser fluence and the number of the laser pulses. The high boron concentration of 10^{20} atoms cc^{-1} which is close to the solubility in silicon is achieved in the p^+-junctions as a result of the high boron diffusivity in the liquid silicon. The boron depth profiles as a function of the laser fluence and the pulse number are studied by SIMS. It is demonstrated that the junction depth can be changed incrementally by varying either the laser fluence or the pulse number N. The latter is a finer adjustment than the former. Experiments also confirm that the 'box-like' p^+-junctions are formed by multiple laser irradiation as long as the induced maximum melting depth is smaller than the boron diffusion length. The optimal pulsed laser SOG doping fluence range is found about 0.6–0.8 J cm^{-2}. Above this range, the dopant profiles are less sharp because the induced melting depth is larger than the boron diffusion length. This melt–solid interface limited diffusion is found as a key factor in the optimization of the ultra-shallow p^+-junction fabrication. Numerical simulations are carried out to compare with the experimental profiles. It is found that, within the available physical picture, the one-dimensional transient thermal and mass transport model agrees reasonably with the experimental results at the first pulse, but deviates gradually as the laser pulse number increases. Possible mechanisms causing this deviation are discussed, including the boron diffusivity and the solid silicon thermal conductivity dependence on the dopant concentration in the heavily doped region during the multiple laser pulses. Further investigation is needed to elucidate these important issues in the complex tran-

sient thermal and mass transport in the thin liquid silicon layer induced by the pulsed laser irradiation.

Acknowledgements—Support from the National Science Foundation under grant no. CTS-9210333 is gratefully acknowledged. X. Zhang thanks Dr F. Ogletree of Lawrence Berkeley Laboratory for SIMS training and helpful discussions on SIMS calibration.

REFERENCES

1. K. K. Ng and W. T. Lynch, The impact of intrinsic series resistance on MOSFET scaling, *IEEE Trans. Electron Devices* **ED-34,** 503–511 (1987).
2. A. Usami, M. Ando, M. Tsunekane and T. Wada, Shallow-junction formation on silicon by rapid thermal diffusion of impurities from a spin-on-source, *IEEE Trans. Electron Devices* **39,** 105–110 (1992).
3. T. M. Liu and W. G. Oldham, Channeling effect of low energy boron implant in (100) silicon, *IEEE Electron Devices Lett.* **EDL-4,** 59–62 (1983).
4. D. Fan, J. Huang and R. J. Jaccodine, Enhanced tail diffusion of ion implanted boron in silicon, *Appl. Phys. Lett.* **50,** 1745–1747 (1987).
5. T. Sands, J. Washburn, R. Gronsky, W. Maszara, D. K. Sadana and G. A. Rozgonyi, Near-surface defects formed during rapid thermal annealing of pre-amorphized and BF_2^+-implanted silicon, *Appl. Phys. Lett* **45,** 982–984 (1984).
6. R. B. Fair, Damage removal/dopant diffusion tradeoffs in ultra-shallow implanted p^+-n junctions, *IEEE Trans. Electron Devices* **ED-37,** 2237–2242 (1990).
7. T. F. Duesch, D. J. Ehrlich, D. D. Rathman, D. J. Silversmith and R. M. Osgood, Electrical properties of laser chemically doped silicon, *Appl. Phys. Lett.* **39,** 825–827 (1981).
8. K. H. Weiner, P. G. Carey, A. M. McCarthy and T. W. Sigmon, An excimer-laser-based nanosecond thermal diffusion technique for ultra-shallow *pn* junction fabrication, *Microelectron. Engng* **20,** 107–130 (1993).
9. K. Sugioka, and K. Toyoda, Generation of carrier concentrations as high as 5×10^{19} cm^{-3} in GaAs by Si doping using a KrF excimer laser, *Appl. Phys. Lett.* **61,** 2817–2819 (1992).
10. A. Slaoui, F. Foulon and P. Siffert, Excimer laser induced doping of phosphorus into silicon, *J. Appl. Phys.* **67,** 6197–6201 (1990).
11. R. G. Wilson, F. A. Stevie and C. W. Magee, *Secondary Ion Mass Spectrometry: a Practical Handbook for Depth Profiling and Bulk Impurity Analysis*, pp. 3.1.1–3.2.4. Wiley, New York (1989).
12. D. R. Atthey, A finite difference scheme for melting problems, *J. Inst. Math. Applics* **13,** 353–366 (1974).
13. N. Shamsundar and E. M. Sparrow, Analysis of multidimensional conduction phase change via the enthalpy model, *J. Heat Transfer* **97,** 333–340 (1975).
14. H. Kodera, Diffusion coefficients of impurities in silicon melt, *Jpn. J. Appl. Phys.* **2,** 212–219 (1963).
15. B. S. W. Kuo, J. C. M. Li and A. W. Schmid, Thermal conductivity and interface thermal resistance of Si film on Si substrate determined by photothermal displacement interferometry, *Appl. Phys. A.* **55,** 289–296 (1992).
16. S. Wolf and R. N. Tauber, *Silicon Processing for the VLSI Era*, Vol. 1, p. 251. Lattice Press, CA (1984).
17. Y. C. Tai, C. H. Mastrangelo and R. S. Muller, Thermal conductivity on heavily doped low-pressure chemical vapor deposited polycrystalline silicon films. *J. Appl. Phys.* **63,** 1442–1447 (1988).
18. G. Slack, Thermal conductivity of pure and impure silicon, silicon carbide and diamond, *J. Appl. Phys.* **35,** 3460–3466 (1964).
19. R. F. Wood and G. E. Jr Jellison, Melting model of the pulsed laser process. In *Semiconductors and Semimetals* (Edited by R. F. Wood and C. W. White), Vol. 23, pp. 165–250. Academic Press, Orlando, FL (1984).